Supplementary Materials for

Molecular basis for high affinity agonist binding in GPCRs

Tony Warne[1], Patricia C. Edwards[1], Andrew S. Doré[2], Andrew G. W. Leslie[1] &
Christopher G. Tate[1]*

Correspondence to: cgt@mrc-lmb.cam.ac.uk

This PDF file includes:

Materials and Methods
Figs. S1 to S9
Tables S1 to S4
Captions for databases S1 and S2

Other Supplementary Materials for this manuscript includes the following:

Data S1 and S2

Materials and Methods

Cloning, expression and purification of β_1AR.

The turkey (*Meleagris gallopavo*) β_1AR construct trx-β_1AR (*12*) used for crystallization of the β_1AR-nanobody complexes was a thioredoxin fusion (trx) based on β44-m23, with the same truncations and deletions, but only four thermostabilizing mutations, R68S$^{1.59}$, M90V$^{2.53}$, F327A$^{7.37}$ and F338M$^{7.48}$. The mutations Y227A$^{5.58}$ and A282L$^{6.27}$ on H5 and H6 were removed, because the reversion of these two mutations was sufficient to enable full activation and high affinity agonist binding in the presence of G proteins and nanobody Nb80 (*17*). The mutation R284K$^{6.29}$ was included to make the cytoplasmic nanobody-binding interface equivalent to that of the β_2AR (*8*). A thioredoxin (*E. coli* trxA, with mutations C32S & C35S) fusion was attached via the linker EAAAK at the N-terminus of β_1AR. The construct was cloned into the baculovirus transfer vector pAcGP67B (BD Biosciences) and the recombinant baculovirus was generated by co-transfection of insect cells with BacPAK6 linearized baculovirus DNA (Oxford Expression Technologies Ltd). Plaque purified virus was used to express receptors in High Five cells (ThermoFisher Scientific) grown in ESF921 (Expression Systems) supplemented with 5% heat-inactivated foetal bovine serum (Sigma) as described previously (*18*).

The membrane fraction was prepared, and the receptor was solubilized in 1.5% decylmaltoside (DM, Generon) and further purified in 0.1% DM by Ni^{2+}-affinity chromatography and alprenolol sepharose chromatography, with elution from the alprenolol sepharose ligand affinity column as described previously (*12, 18, 19*) with 100

µM of the appropriate ligand for complex formation, concentrated to 15-25 mg/ml and either used directly for the formation of complexes, or frozen for later use.

Expression and purification of nanobodies Nb80 and Nb6B9. Synthetic genes (Integrated DNA Technologies) for Nb80 (*8*) and Nb6B9 (*10*) were cloned into plasmid pET-26b(+) (Novagen) with a N-terminal His$_6$ tag followed by a thrombin protease cleavage site. Expression in *E. coli* strain BL21(DE3)RIL (Agilent Technologies) and purification from the periplasmic fraction were as described elsewhere (*10*), but with the addition of a final thrombin (Sigma) protease cleavage step to remove the His$_6$ tag before concentration to 40 mg/ml.

Formation of agonist-bound trx-β$_1$AR-nanobody complexes and purification with detergent exchange by size exclusion chromatography (SEC).

Trx-β$_1$AR (1.0-2.0 mg) was mixed with 1.5-fold molar excess nanobody (0.4-0.8 mg) with the addition of cholesteryl hemisuccinate (Sigma) to 0.1 mg/ml in a final volume of 150 µL. For the formation of activated complexes with receptor purified in full agonist (isoprenaline), Nb80 was used and incubation was for 2 hours at room temperature. For the formation of complexes with receptor purified in partial agonists (salbutamol, dobutamine and cyanopindolol), trx-β$_1$AR was mixed with Nb6B9 and incubated overnight at room temperature. After incubation, size exclusion chromatography (SEC) was performed to separate receptor-nanobody complexes from excess nanobody and to exchange the detergent from DM to HEGA-10 for crystallization

by vapour diffusion. A Superdex Increase 200 10/300GL column (GE) was used at 4°C, the column was equilibrated with SEC buffer (10 mM Tris-HCl pH 7.4, 100 mM NaCl, 0.1 mM EDTA, 0.35% HEGA-10 [Anatrace]) supplemented with 10 μM of the appropriate agonist ligand. Samples containing complex were mixed with 200 μL SEC buffer and centrifuged (14,000 x g, 5 minutes) immediately prior to SEC (flow rate 0.2 ml/minute), with a run time of one hour which was sufficient for a near-complete detergent exchange as indicated by quantitation of residual glycosidic detergent (20). Peak fractions corresponding to complex were concentrated to 15 mg/ml for crystallization by vapour diffusion using Amicon Ultra-4 50 kDa centrifugal filter units (EMD-millipore).

Crystallization of receptor-nanobody complexes, data collection, processing and refinement.

Crystals were grown in 150 nL + 150 nL sitting drops by vapour diffusion at 18°C against reservoir solutions containing 0.1 M Hepes-NaOH pH 7.5 and 21-24% PEG1500; the yield of crystals was increased by addition of HEGA-10 to 0.5-0.6% prior to setting up the drops. Crystals usually appeared within 2 hours and grew to full size (up to 200 μm in length) within 48 hours. Crystallization plates were equilibrated to 4°C for at least 24 hours before cryo-cooling. Crystals were picked in LithoLoops (Molecular Dimensions Ltd) and transferred to 0.1 M Hepes-NaOH pH 7.5, 25% PEG1500 containing 5% glycerol for 2 seconds before plunging into liquid nitrogen.

Diffraction data for trx-β$_1$AR-nanobody complex crystals were collected at ESRF, Grenoble using beamlines id23-2, id30-a3, id29 & id30b. Helical collection strategies

were used to collect complete data sets while translating between two points in order to minimize radiation damage. The thioredoxin fusion was not well resolved in the structures and the linker to the receptor's N-terminus were not modeled, but the fusion it was important for ease of data collection as it resulted in crystals with an orthorhombic space group and not monoclinic as is usual when β_1AR is crystallized in Hega-10 (*12*). Diffraction data were processed using MOSFLM (*21*) and AIMLESS (*22*), structures were solved using PHASER (*23*) with use of the crystal structures of the active state β_2AR stabilized with nanobody Nb80(*8*) and wild-type thioredoxin (PDBs 3P0G and 2H6X) as search models. Diffraction was significantly anisotropic, as can be seen from the estimated resolution limits (based on a $CC_{1/2}$ value of 0.3) in the h,k,l directions (Table S1). In order to preserve the statistically significant diffraction data in the well-diffracting directions in reciprocal space, while eliminating reflections in the less well-diffracting directions that contained no useful information, the data were subjected to anisotropic truncation using STARANISO (http://staraniso.globalphasing.org) or the UCLA Diffraction Anisotropy Server (http://services.mbi.ucla.edu/anisoscale/). This inevitably leads to both low overall completeness (52-66%) and in particular very low completeness (2.8-12.6%) in the outermost resolution bin (Table S1). Model refinement and rebuilding were carried out with REFMAC5 (*24*) and COOT (*25*).

Expression and purification of mini-G$_s$.

Mini-G$_s$ (construct 393) was expressed in *E. coli* strain BL21(DE3)RIL and purified by Ni^{2+}-affinity chromatography, followed by cleavage of the histidine tag using TEV protease and negative purification on Ni^{2+}-NTA to remove TEV and undigested

mini-G_s; SEC was then used to remove aggregated protein as described elsewhere (*26*). Purified mini-G_s was concentrated to give a final concentration to 100 mg/ml in 10 mM HEPES, pH 7.5, 100 mM NaCl, 10% v/v glycerol, 1 mM $MgCl_2$, 1 μM GDP and 0.1 mM TCEP.

Preparation of activated trx-$β_1$AR-mini-Gs complexes.

For the comparison of complex formation with mini-G_s in the presence of either full or weak partial partial agonist, 150 μM trx-$β_1$AR was incubated overnight at 4°C with 200 μM mini-G_s in a final volume of 200 μL SEC buffer (10 mM Tris-HCl pH7.4, 100 mM NaCl, 1 mM $MgCl_2$, 0.1% DM) containing 0.75 mM ligand (either isoprenaline or cyanopindolol). A further 1 hour incubation followed addition of 0.1 unit apyrase (Sigma), after which the sample was centrifuged (14,000 x*g*, 5 minutes) before SEC using a Superdex Increase 200 10/300GL column (GE) at 4°C. The column was run at 1 ml/minute in SEC buffer with the addition of 10 μM ligand, and 0.8ml fractions were collected for analysis by SDS-PAGE. The results of these experiments are shown in Fig. S7, and indicate that in the presence of weak partial agonist, the trx-$β_1$AR-mini-G_s complex is unstable, and therefore G protein mimetic nanobodies Nb80 or Nb6B9 were used in this study to prepare crystals with a range of ligands with differing pharmacological profiles.

Radioligand binding studies on βARs and mutants.

Wild type turkey $β_1$AR, human $β_1$AR and human $β_2$AR, and mutants of these receptors, were all expressed using recombinant baculoviruses in insect cells for

6

radioligand binding studies. Amino acid residues close to the ligand binding pocket (LBP) which differ between turkey β_1AR and β_2AR were mutated to compare some of the pharmacological characteristics of the different receptor subtypes. The residues selected for mutation were Trp182^{ECL2}, Asn313$^{6.58}$, Asp322$^{7.32}$ and Phe325$^{7.35}$ in turkey β_1AR, which are equivalent to Tyr174^{ECL2}, His296$^{6.58}$, Lys305$^{7.32}$ and Tyr308$^{7.35}$ in β_2AR. The first residues, Trp182^{ECL2}/Tyr174^{ECL2} (β_1AR/β_2AR) was chosen because they are involved in differing modes of interaction with Phe201^{ECL2}/Phe193^{ECL2} that were observed in comparisons of crystal structures, as well as possible involvement in a secondary affinity state observed in β_1AR but not β_2AR(*27*). The latter three pairs of residues were chosen because His296$^{6.58}$, Lys305$^{7.32}$ and Tyr308$^{7.35}$ have all been suggested to contribute to high affinity binding of agonist to β_2AR in the presence of G protein (*10, 14*). For further details, see Fig S8.

The initial turkey β_1AR construct was based on the β44-m23 construct (*12*), but without any of the stabilizing mutations. Two variants of β_1AR were prepared with mutations of amino acids in the ligand binding pocket (LBP) that were intended to make the β_1AR similar to the β_2AR. These were β_1AR(F325Y) (mutation F325Y$^{7.35}$) and β_1AR(β_2LBP) that contained following mutations: W182Y^{ECL2}, N313H$^{6.58}$, D322K$^{7.32}$, F325Y$^{7.35}$. The human β_2AR was mutated to generate the construct β_2AR(β_1LBP) that contained the mutations Y174W^{ECL2}, H296N$^{6.58}$, K305E$^{7.32}$ and Y308F$^{7.35}$. Mutants were constructed in the baculovirus transfer vectors pBacPAK8 (Clontech) for β_1AR and pAcGP67B (BD Biosciences) for β_2AR(β_1LBP) by using Quikchange protocols (Stratagene) with KOD polymerase (EMD Millipore), and were expressed in insect cells after co-transfection with linearized baculovirus as previously described. Crude insect

cell membrane fractions were prepared by resuspending cell pellets from 1 ml culture volume in 1 ml of assay buffer (20 mM Hepes-NaOH pH 7.5, 50 mM NaCl, 2.5 mM MgCl$_2$, 0.1% BSA) to give final concentrations of 1-3 x 10^6 cells/ml. Cells were sheared by 10 passages through a bent 26G needle and cell debris was removed by centrifugation (1500 x g, 2 min) and the supernatants were diluted in assay buffer for radioligand binding studies.

Saturation binding assay to determine affinities for [^{3}H]-dihydroalprenolol and [^{125}I]-cyanopindolol.

Saturation binding assays were performed on all constructs to determine appropriate apparent K$_D$ values for [^{3}H]-dihydroalprenolol (DHA) to use in competition binding assays. Insect cell membranes containing βAR constructs were diluted in 20 mM Hepes-NaOH pH 7.5, 50 mM NaCl, 2.5 mM MgCl$_2$, 1 mg/ml BSA. The sample was aliquoted and dilutions of [^{3}H]-DHA (Perkin Elmer) were added to give final concentrations in the range of 0-20 nM (β$_1$AR constructs) and 0-2.5nM (β$_2$AR constructs) in a final volume of 220 μL, with 10 determinations in duplicate per binding curve. Non-specific binding was determined by addition of alprenolol to negative controls (1 mM final concentration). Samples were incubated at 20°C for 2 h, before filtering 100 μL duplicate aliquots through 96-well Multiscreen HTS GF/B glass fibre filter plates (Merck Millipore) pre-soaked in 0.1% w/v polyethyleneimine to separate bound from unbound [^{3}H]-DHA. Filters were then washed three times with 200 μL volumes ice-cold assay buffer (20 mM Hepes-NaOH pH 7.5, 50 mM NaCl, 2.5 mM MgCl$_2$). Filters were dried, punched into scintillation vials and 4 ml Ultima Gold scintillant (Perkin Elmer) were

added. Radioligand binding was quantified by scintillation counting using a Tri-Carb Liquid Scintillation Analyser (Perkin Elmer) and apparent K_D values were determined using GraphPad Prism version 7.0b (GraphPad Software, San Diego, CA). Apparent K_D values were determined for all constructs, also in the presence of 25 μM mini-G_s (R393), in which case apyrase (0.1 U/ml final concentration) was included. All K_D values obtained are given in Tables S2 and S3, and are mean values obtained from at least two experiments performed in duplicate. Mean K_D values for [^{125}I]-cyanopindolol (Cyp) were also determined for $β_1$AR using a concentration range of 0-1000 pM [^{125}I]-Cyp, with non-specific binding determined by addition of cyanopindolol to negative controls (0.1 mM final concentration).

Competition binding assays.

Insect cell membranes containing βAR were resuspended in assay buffer (20 mM HEPES pH 7.5, 50 mM NaCl, 2.5 mM $MgCl_2$, 0.1% BSA, with inclusion of 0.1 mM ascorbate for ligands containing catechols). The sample was aliquoted and mini-G_s construct R393 (25 μM final concentration, for determination of high affinity states), agonist (8 points with final concentrations in the range of 1 pM–10 mM) and apyrase (0.1 U/ml final concentration) were added to give a final volume of 220 μL. Non-specific binding was determined by addition of alprenolol to the negative control (100 μM final concentration). Samples were incubated at 20°C for 1 h, before adding [^{3}H]-DHA (concentrations of the competing ligand were varied depending on the apparent K_D determined for the construct with and without G protein (see Table S3), so that concentrations of competing ligand were in the range 1-2.5 x K_D). Samples were

9

incubated at 20°C for 1-5 h (longer incubation times were required for the wild-type β_2AR to allow equilibration with DHA), before filtering through 96-well fibre filter plates as previously described. Radioligand binding was quantified by scintillation counting and K_i values were determined using GraphPad Prism version 7.0b. All K_i values obtained are given in Tables S2 and S3 and are mean values obtained from at least two experiments performed in duplicate. Racemic mixtures of the tested ligands were used in all cases apart from measurements with epinephrine and norepinephrine where the active (*R*-) enantiomers were used, and also dobutamine where the chiral β-OH is not present. Where racemic mixtures were used, ligand concentrations and K_i values were not corrected for the presence of the inactive enantiomers

Radioligand association experiments.

Assays were performed using insect cell membranes containing βAR resuspended in assay buffer (20 mM HEPES pH 7.5, 50 mM NaCl, 2.5 mM $MgCl_2$, 0.1% BSA). For β_1AR, [^{3}H]-DHA association time course experiments were performed at 4°C, reactions were initiated by dilution of insect cell membranes into [^{3}H]-DHA to give final concentrations of approximately 8-10 fold K_D for DHA (final concentrations: β_1AR, 10 nM, β_1AR(F325Y) 8.3 nM, β_1AR(F325A), 10.5 nM). Aliquots (50 µL) were withdrawn at the indicated times and filtered to separate bound from unbound [^{3}H]-DHA using Whatman GF/B filters which were further processed as described previously. Experiments were performed in triplicate, with non-specific binding determined by addition of alprenolol to negative controls (1 mM final concentration). Comparisons of relative accessibilities of the ligand binding pocket (LBP) of different βAR subtypes and mutants in the presence of mini-G_s were performed at room temperature with [^{125}I]-

cyanopindolol (Cyp). Samples of receptor (0.06-0.08 nM in final volume 108 µL with and without mini-G$_s$ [27.8µM]) were incubated for at least 2 hours at room temperature before addition of 12 µL [^{125}I]-Cyp to final concentrations that varied from 750-980 pM. After allowing 1.25 h for binding of [^{125}I]-Cyp, 50 µL aliquots were withdrawn and bound [^{125}I]-Cyp was separated from unbound by filtration with Whatman GF/B filters. Relative accessibility of the LBP was calculated as a percentage of [^{125}I]-Cyp binding, mean values were calculated from 6-7 separate experiments for each construct and are displayed in Table S4.
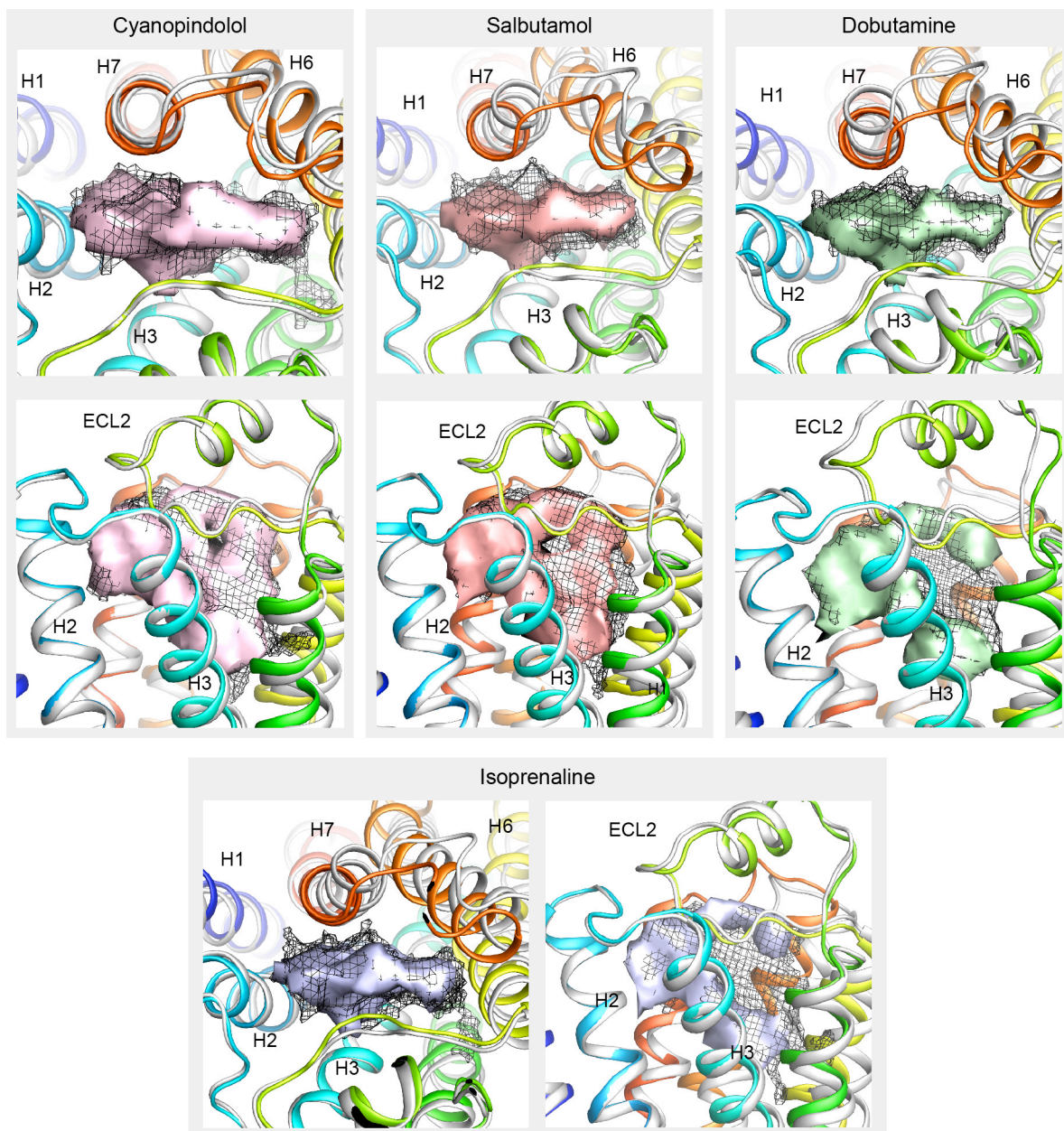
Fig. S1.

Volume differences of the orthosteric binding site between the inactive state and active state. In each panel β_1AR is shown as a cartoon (inactive state, grey; active state, rainbow coloration, N-terminus blue, C-terminus red). The volume of the inactive state is outlined as a mesh and the volume of the active state is outlined as a solid surface. The two views are from the extracellular surface and parallel to the membrane plane.
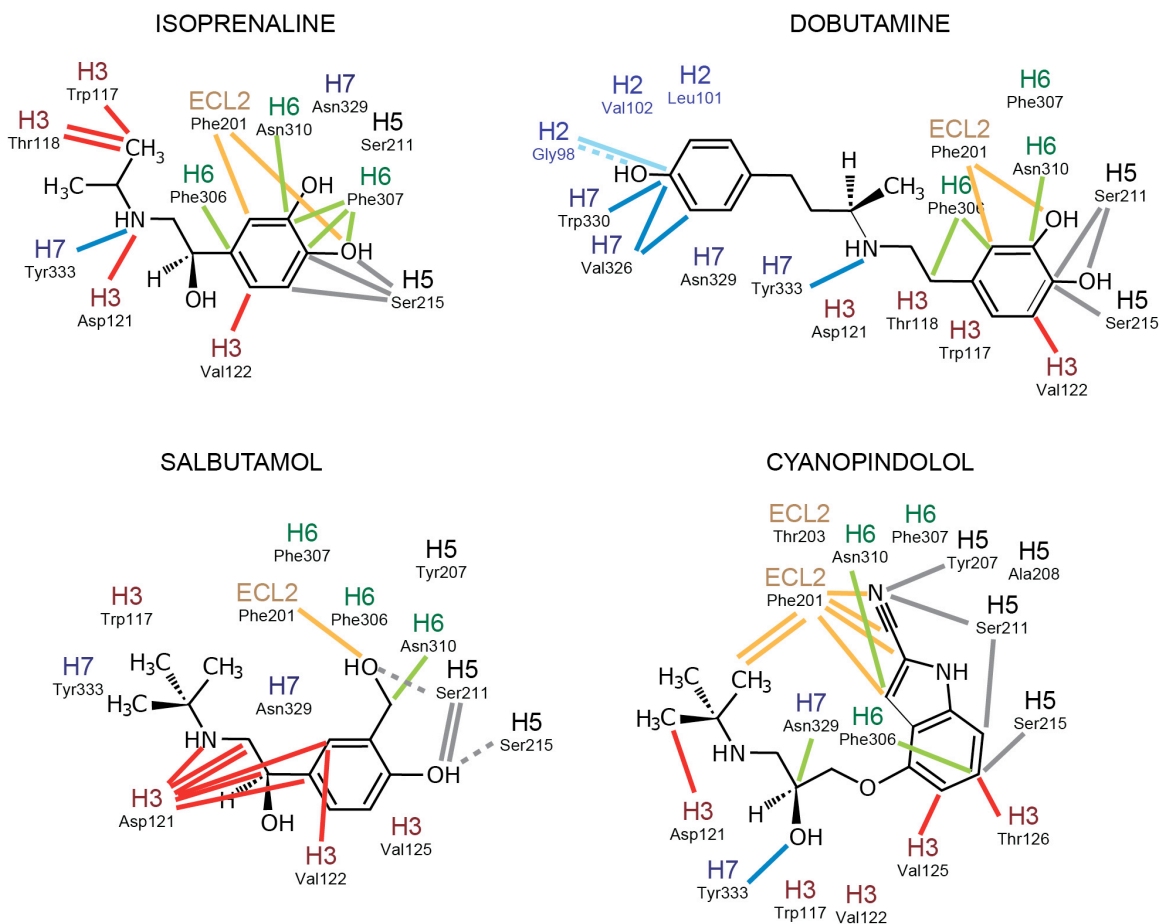
Fig. S2.

Additional contacts between β₁AR and ligands in the active state. Structures of agonists co-crystallized with β₁AR are shown and depicted with receptor-ligand contacts present in the active state but absent in the inactive state: solid lines, van der Waals interactions (≤ 3.9 Å), dashed line, polar interaction. Colors represent the α-helices or extracellular loops where each residue is located and correspond to the colors in Fig. 2 and Fig. 3. If no lines are present between a residue and the ligand, contacts are present in both the inactive state and active state, but no additional contacts formed upon receptor activation.
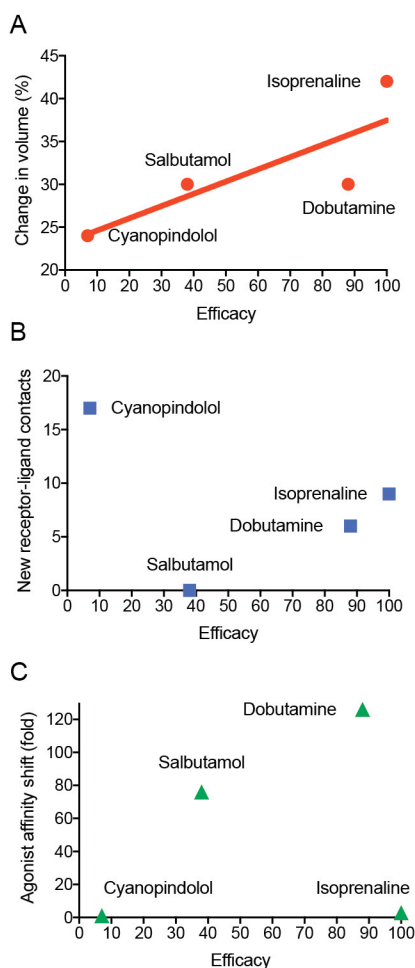
Fig. S3.

Correlation between structural changes in active state GPCRs and ligand efficacy. Ligand efficacies used are for the crystallization construct without thermostabilising mutations and thioredoxin fusion (construct β36; (*28*)). In this context, efficacy is defined as the percentage of the maximal response of the ligands compared to the isoprenaline response, obtained from ^{3}H-cAMP accumulation assays in a stable CHO cell line expressing β36 (*28*). (A) Relationship between efficacy and the change in volume of the orthosteric binding site. Linear regression (r^2=0.62) gives a best fit line that is not statistically significant. If only similar chemotypes are considered (cyanopindolol, salbutamol, isoprenaline) linear regression gives a perfect straight line. Dobutamine differs from these three ligands in having a large amine substituent that binds outside the canonical ligand binding pocket and it also lacks the β-hydroxyl moiety. (B) Relationship between efficacy and the number of additional ligand-receptor atomic contacts generated upon formation of the active state. (C) Relationship between efficacy and the degree of affinity change between the inactive state and active state.
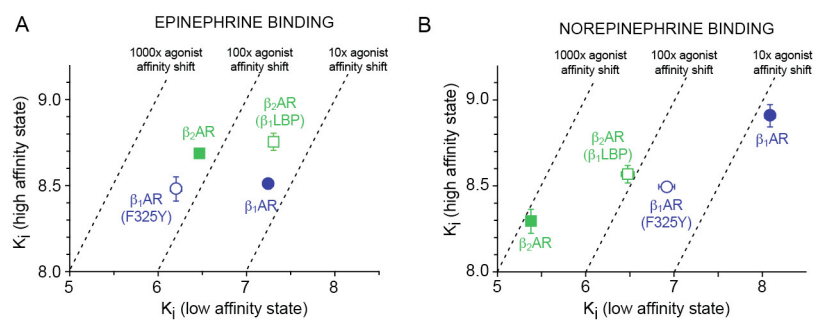
14

Fig. S4.

Affinities of β₁AR and β₂AR mutants in the high and low affinity states. (A, B) Comparison of the affinities for agonist binding in the high affinity state and the low affinity state in relation to the agonist affinity shift; β₁AR, blue filled circles; β₁AR(F325Y), blue open circles; β₂AR green filled squares; β₂AR(β₁LBP), green open squares (Tables S2 and S3; Figure S6). All data are in Tables S2 and S3, and representative graphs of affinity shifts are in Figure S6. Results are the mean of 2-7 experiments performed in duplicate with error bars representing the SEM.
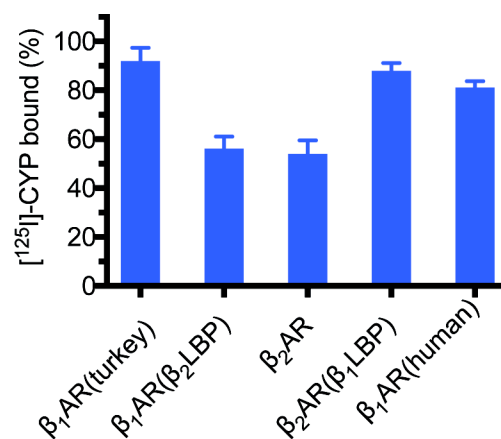
Fig. S5.

Accessibility of the orthosteric binding pocket to ^{125}I-cyanopindolol of β_1AR and β_2AR. The amount of ^{125}I-cyanopindolol (^{125}I-Cyp) that associated with receptor-mini-G_s complexes after a 75 minute incubation (see Methods) was determined in relation to the amount of ^{125}I-Cyp bound to the respective receptor in the absence of mini-G_s. Data represent the mean of 6-7 independent experiments performed in duplicate.

Fig. S6.

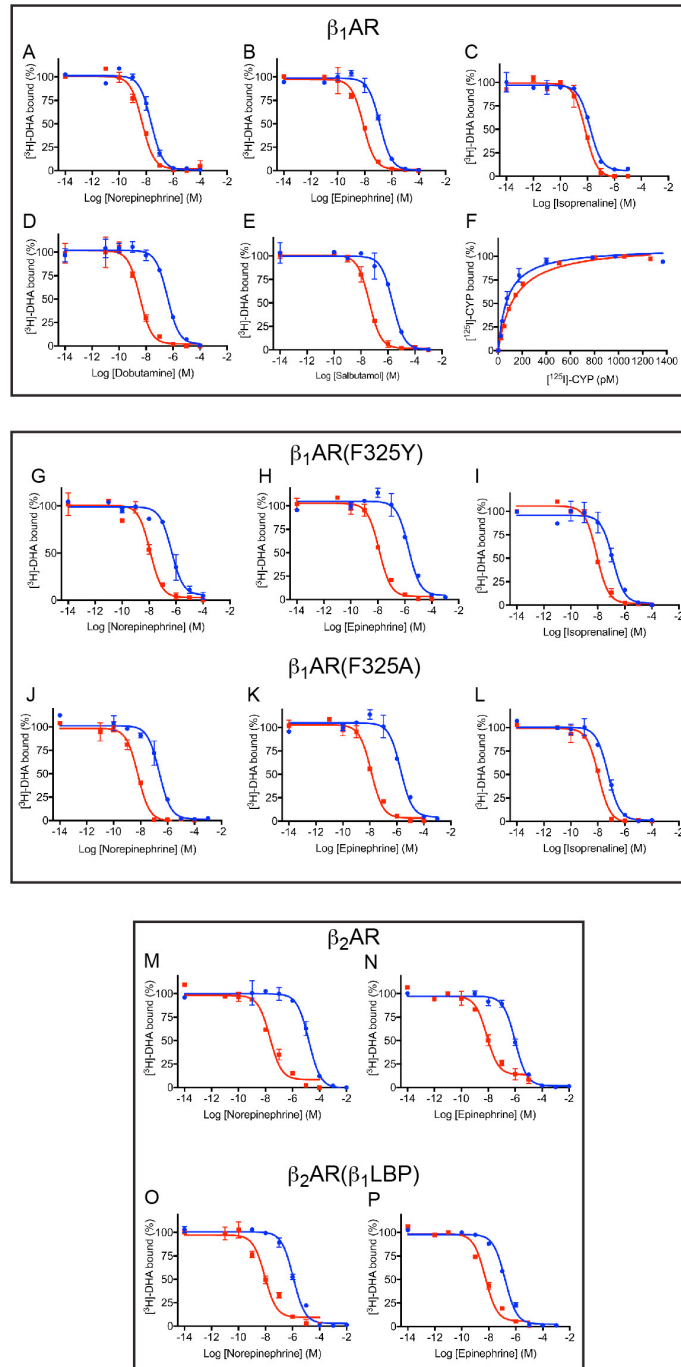**Pharmacology of high affinity and low affinity states.** Representative competition binding curves and saturation binding curves are shown for results in Tables S2 and S3. All experiments were performed in duplicate. Experiments to determine the high affinity state were performed in a molar excess of mini-G_s (see Methods); red curves, low affinity state; blue curves, high affinity state.
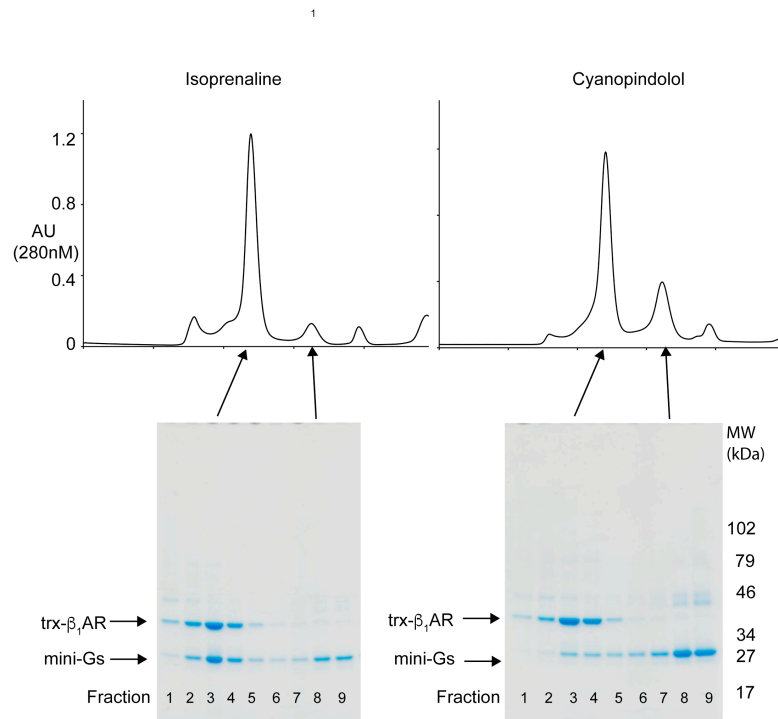
Fig. S7.

Formation of complexes between trx-β₁AR and mini-Gₛ in the presence of isoprenaline or cyanopindolol. Complexes were formed as described in the Methods section in the presence of either the full agonist isoprenaline or the weak partial agonist cyanopindolol. The components were then resolved by SEC and the fractions analysed by Coomassie blue-stained SDS-PAGE.
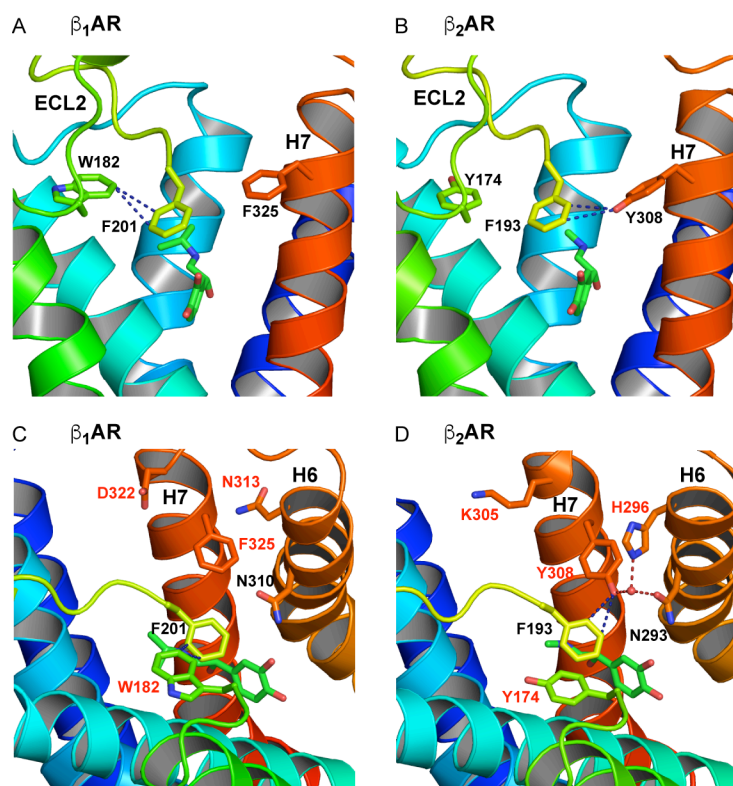
Fig. S8.

Comparison of β₁AR and β₂AR structures: subtype-specific differences imply rationale for mutagenesis. Comparison of structures of (a) activated β₁AR with isoprenaline bound and (b) β₂AR with adrenaline bound (4LDO). In β₁AR, F201 interacts with W182 on ECL2, and not F325 on H7, in the β₂AR F193 interacts with Y308 on H7, but not with Y174 on ECL2. This subtype specific difference in interactions between F201 (β₁AR) and F193 (β₂AR) can be observed in most structures with the exception of β₂AR crystallized with ligands with bulky headgroups, where interactions between F193 and Y174 can be observed. Alternative views of activated β₁AR with isoprenaline bound (c) and (d) β₂AR with adrenaline bound (4LDO) with ECL2 removed for clarity, residues that differ between the two receptors are labeled in red. In the β₂AR, of these, H296, K305 & Y308 have been suggested as being involved in high affinity agonist binding states. In the case of H296, this is by participation in an extended H-bond network that also includes T195 on ECL2 (not shown).

ISOPRENALINE

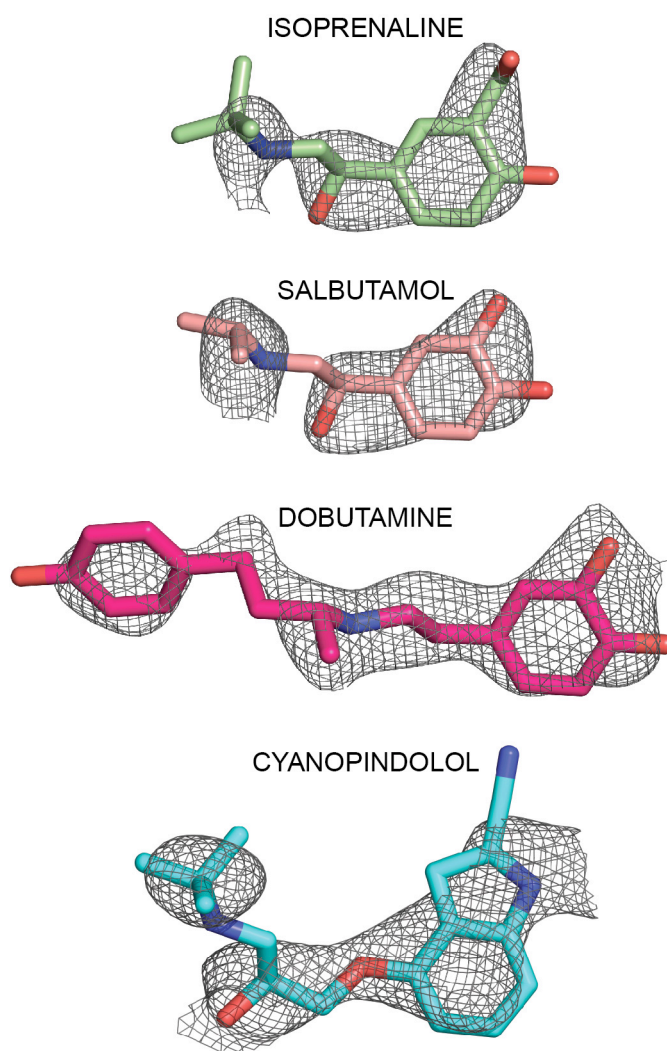SALBUTAMOL

DOBUTAMINE

CYANOPINDOLOL

Fig. S9.
2Fo-Fc omit maps (1.2σ mesh) for ligands

Table S1. X-ray data collection and refinement statistics

Ligand, nanobody	Isoprenaline, Nb80	Salbutamol, Nb6B9	Dobutamine, Nb6B9	Cyanopindolol, Nb6B9
ESRF beamlines	id23-2	id30b	id30-a3 & id29	id30-a3
Number of crystals	1	2	4	2
Space group	P 2_1 2_1 2_1	P 2_1 2_1 2_1	P 2_1 2_1 2_1	P 2_1 2_1 2_1
Cell dimensions *a, b, c* (Å)	116.7, 121.2, 129.5	116.6, 121.5, 130.4	116.5, 119.7, 129.2	116.6, 120.0, 130.1
Resolution range[1]	41.38-2.78 (2.88- 2.78)	25.77-2.61 (2.68-2.61)	41.08-2.7 (2.79-2.7)	38.22-2.79 (2.89-2.79)
Unique reflections[1]	46114 (3946)	56733 (4129)	50091 (4298)	45172 (3688)
Completeness before truncation (%)[1]	98.5 (87.2)	99.0 (89.3)	99.4 (94.1)	98.3 (82.9)
Multiplicity[1]	9.1 (6.4)	9.5 (6.2)	15.8 (8.6)	9.8 (3.7)
Mean isotropic I/σI before truncation[1]	5.1 (0.0)	5.0 (0.3)	4.9 (0.5)	3.7 (0.2)
R-merge[1]	0.408 (-71.6)	0.334 (6.69)	0.553 (6.61)	0.378 (5.28)
R-pim[1]	0.206 (-42.91)	0.166 (4.272)	0.204 (3.40)	0.18 (4.53)
Resolution limits CC1/2=0.3 h, k, l axes & *overall* (Å)	2.78, 3.72, 3.24, ***3.06***	2.67, 3.47, 3.42, ***3.01***	2.7, 3.99, 3.44, ***3.06***	2.91, 4.24, 3.63, ***3.2***
REFINEMENT				
Resolution (Å)[1]	41.4-2.8 (2.873-2.8)	25.8-2.76 (2.83-2.76)	41.1-2.7 (2.77-2.7)	38.2-2.8 (2.87-2.8)
Completeness, truncated data (%)[1]	64.9 (9.0)	66.8 (3.9)	58.7 (12.6)	52.1 (2.9)
No. reflections	28351	30724	28040	23793
R-work/R-free (%)[1]	0.284/0.317 (0.333/0.392)	0.265/0.285 (0.427/0.324)	0.241/0.278 (0.452/0.412)	0.240/0.274 (0.496/0.703)
No. atoms	8094	8231	8280	8190
Protein	7934	8015	8014	7977
Ligands & detergents	140	203	252	206
Water	20	13	14	7
B-factors (Å^2)				
Protein	74	84	65	83
Ligand & detergents	55, 54	64, 77	57, 68	56, 78
Waters	38	41	24	39
Wilson B-factor	80	97	58	65
R.M.S.D.				
Bond lengths (Å)	0.008	0.008	0.008	0.008
Bond angles (°)	1.12	1.2	1.18	1.11

[1]Values in parentheses are for the highest resolution shell.

Table S2.

Affinities (K_i values) of β_1AR and β_2AR constructs for ligands

Receptor and construct	Ligand	K_i low affinity state (Log)	SEM	n	K_i high affinity state (Log)	SEM	n	Affinity shift (Log)	Affinity shift (fold)
β_1AR	Isoprenaline	-8.16	0.01	2	-8.62	0.02	2	0.46	2.9
$\beta_1AR(F325Y)$	Isoprenaline	-7.28[1]	0.05	2	-8.69[2]	0.01	2	1.27	18.7
$\beta_1AR(F325A)$	Isoprenaline	-7.68[1]	0.02	2	-8.59[2]	0.08	2	0.9	8
β_1AR	Salbutamol	-5.92	0.06	3	-7.80	0.06	3	1.88	76
β_1AR	Dobutamine	-6.86	0.03	4	-8.97	0.03	4	2.10	126
β_1AR	Norepinephrine	-8.09	0.06	4	-8.91	0.07	4	0.82	6.6
$\beta_1AR(F325Y)$	Norepinephrine	-6.92[3]	0.09	6	-8.49[4]	0.06	4	1.58	38
$\beta_1AR(F325A)$	Norepinephrine	-7.09[3]	0.05	2	-8.76[5]	0.01	2	1.67	46.4
β_1AR	Epinephrine	-7.25	0.06	5	-8.51	0.03	6	1.27	18
$\beta_1AR(F325Y)$	Epinephrine	-6.20[6]	0.06	4	-8.48[7]	0.07	4	2.28	189
$\beta_1AR(F325A)$	Epinephrine	-6.56[6]	0.05	2	-8.45[7]	0.03	2	1.89	77.8
β_2AR	Norepinephrine	-5.38	0.05	4	-8.29	0.07	7	2.91	818
$\beta_2AR(\beta_1LBP)$	Norepinephrine	-6.48[8]	0.07	3	-8.57[9]	0.05	5	2.09	124
β_2AR	Epinephrine	-6.47	0.03	6	-8.69	0.02	5	2.22	166
$\beta_2AR(\beta_1LBP)$	Epinephrine	-7.31[10]	0.01	2	-8.76[11]	0.05	2	1.45	28

[1,3,4,6] Significant difference between value of K_i and the value obtained with β_1AR and the same ligand
[2,5,7] No significant difference between value of K_i and the value obtained with β_1AR and the same ligand
[8,9,10] Significant difference between value of K_i and the value obtained with β_2AR and the same ligand
[11] No significant difference between value of K_i and the value obtained with β_2AR and the same ligand
Significance was determined using an unpaired t test, $P<0.05$.

Table S3.

Apparent K_D values of β_1AR and β_2AR constructs for cyanopindolol and dihydroalprenolol

Receptor and construct	Ligand	K_D control (Log)	SEM	n	K_D + mini-G_s (Log)	SEM	n	Affinity shift (Log)	Affinity shift (fold)
β_1AR	$[^{125}I]$-cyanopindolol	-9.99	0.03	4	-9.85	0.02	4	-0.14	-0.72
β_1AR	$[^3H]$-DHA	-8.87	0.08	5	-9.47	0.05	5	n/a	n/a
$\beta_1AR(F325Y)$	$[^3H]$-DHA	-9.03	0.01	2	-9.60	0.05	2	n/a	n/a
$\beta_1AR(F325A)$	$[^3H]$-DHA	-8.96	0.01	2	-9.77	0.04	5	n/a	n/a
β_2AR	$[^3H]$-DHA	-9.66	0.09	3	-10.19	0.03	3	n/a	n/a
$\beta_2AR(\beta_1LBP)$	$[^3H]$-DHA	-9.48	0.09	4	-9.88	0.03	2	n/a	n/a

Table S4.

Association of ^{125}I-Cyp to active state receptors

Receptor and construct	^{125}I-Cyp bound[1] (%)	SEM	n
β_1AR (turkey)	91.6	5.8	6
β_1AR(β_2LBP)	55.9	5.2	7
β_2AR	53.7	5.9	6
β_2AR(β_1LBP)	87.7	3.5	7
β_1AR (human)	80.8	2.9	7

Data S1. (separate file)

Atomic contacts between receptor and ligands

Data S2. (separate file)

Ligand-receptor distance differences